Synthesis of Hierarchical BiOBr Nanostructure Flowers by PVP-Assisted Hydrothermal Method and Their Photocatalytic Activities

ANUKORN PHURUANGRAT [1,5] SOMCHAI THONGTEM,[2,3] and TITIPUN THONGTEM[3,4,6]

1.—Department of Materials Science and Technology, Faculty of Science, Prince of Songkla University, Hat Yai, Songkhla 90112, Thailand. 2.—Department of Physics and Materials Science, Faculty of Science, Chiang Mai University, Chiang Mai 50200, Thailand. 3.—Materials Science Research Center, Faculty of Science, Chiang Mai University, Chiang Mai 50200, Thailand. 4.—Department of Chemistry, Faculty of Science, Chiang Mai University, Chiang Mai 50200, Thailand. 5.—e-mail: phuruangrat@hotmail.com. 6.—e-mail: ttpthongtem@yahoo.com

Hierarchical BiOBr nanostructure flowers as a visible-light-driven photocatalyst were synthesized by the polyvinylpyrrolidone (PVP)-assisted hydrothermal process. The role of PVP content on product morphologies and photocatalytic activities for photodegradation of rhodamine B (RhB) under visible light irradiation was studied. The as-synthesized nanostructure BiOBr samples were characterized by x-ray diffraction (XRD), Fourier transform infrared spectroscopy (FTIR), Raman spectrophotometry, scanning electron microscopy (SEM), transmission electron microscopy (TEM) and x-ray photoelectron spectroscopy. XRD patterns of the products were used to identify the well-defined pure tetragonal BiOBr phase. SEM and TEM images showed that the as-synthesized BiOBr without PVP adding was uniform square BiOBr nanoplates with edge length of 1–3 μm. Upon adding 1.00 g of PVP 10 kDa, the uniform square BiOBr nanoplates were transformed into hierarchical BiOBr nanostructure flowers with a size of 3–4 μm. FTIR and Raman spectra of hierarchical BiOBr nanostructure flowers were used to reveal the presence of Bi-O and Bi-Br stretching vibration modes. The photocatalytic activity of hierarchical BiOBr nanostructure flowers was 96.10% degradation of RhB under visible light within 180 min. Formation mechanism of hierarchical BiOBr nanostructure flowers was also proposed according to the experimental results.

Key words: BiOBr, hierarchical nanostructure flowers, photocatalysis, spectroscopy

INTRODUCTION

In recent years, the main pollutants from organic dyes, cosmetic products and pigments are serious problems and hazardous to organisms and human health.[1–3] Advanced oxidation processes (AOPs) as efficient and green methods of all chemical and biological processes used to completely eliminate and mineralize most organic pollutants by transforming them into less harmful compounds are very interesting because they are inexpensive processes and can be operated under ambient conditions with short reaction time.[4–6] During processing, active radicals such as hydroxyl radicals (˙OH) and superoxide anion radicals (˙O_2^-) are able to completely degrade organic contaminants by converting them into H_2O and CO_2.[4–6]

Bismuth oxyhalides have been intensively investigated because they have excellent electrical, mechanical, photocatalytic and optical properties.[1,7,8] Among them, bismuth oxybromide (BiOBr) as a V–VI–VII ternary compound has received considerable attention for visible-light-driven photocatalytic performance due to its narrow energy bandgap of 2.72 eV for responding in visible light region and a low photo-induced electron–hole recombination rate.[9–11] BiOBr is built of $[Bi_2O_2]^{2+}$ layers interleaved between double layers of Br atoms which can reduce photo-generated electron and hole recombination rates and increase photocatalytic activity.[1,8,9,11] Different morphologies of BiOBr were successfully synthesized such as nanosheets,[1] nanoparticles,[2,3] nanoplates,[3] microspheres,[7,8,11] hollow microspheres,[9] hierarchical microcubes,[10] hierarchical flowers,[12,13] etc. Hierarchical BiOBr nanostructure flowers have high active specific surface areas. Thus, they have photocatalytic activity higher than other morphologies.[12,13]

The hydrothermal method is an inexpensive simple one-step process and is able to apply to larger scale synthesis of BiOBr nanostructure[11,14–16] as compared to other methods such as thermal evaporation,[17,18] alcoholysis-coating method,[19] ultrasonic-assisted method[20] and electrophoretic deposition.[21] Polyvinylpyrrolidone (PVP) as hydrophilic polymer is added to a hydrothermal system to control the morphology of a material. PVP is a non-toxic reagent which has excellent bio-compatibility.[22–24] It can control shape and size of nanostructure BiOBr that leads to improved photocatalytic activity for degradation of dyes and toxic organic compounds in wastewater.[23,24]

In this research, polyvinylpyrrolidone (PVP) with molecular weight of 10,000 (10 kDa) was used as a template for hydrothermal synthesis of hierarchical BiOBr nanostructure flowers. The hierarchical BiOBr nanostructure flowers showed excellent photocatalytic activity for degradation of rhodamine B (RhB) solution under visible light irradiation ($\lambda \geq 420$ nm) of a Xe lamp.

EXPERIMENT

The 0.005 mol of $Bi(NO_3)_3 \cdot 6H_2O$ and NaBr were dissolved in 100 mL deionized water under stirring at room temperature for 30 min. The pH of solutions was adjusted to 6 by 5% NH_4OH under continued stirring. Different contents (0.00 g, 0.10 g, 0.25 g, 0.50 g and 1.00 g) of polyvinylpyrrolidone (PVP 10 kDa) with average molecular weight 10,000 and 1.00 g PVP-35 kDa were added to the solutions with 60 min stirring. The solutions were put in 200 mL home-made stainless steel autoclaves which were heated in an electric oven at 180°C for 24 h. In the end, white precipitates were synthesized, separated by filtering, washed with de-ionized water and ethanol to remove the residual PVP and ions such as Na^+ and NO_3^-, and dried in an electric oven at 80°C for 24 h for further characterization by x-ray diffraction (XRD, Philips X'Pert MPD) with Cu K_α in the 2θ range of 10°–60° at 20 kV and 15 mA. Scanning electron microscopy (SEM) was operated on a JEOL JSM 6335F SEM at 15 kV. Transmission electron microscopy (TEM) was operated on a JEOL JEM 2010 TEM at 200 kV. Fourier transform infrared (FTIR) spectroscopy was carried out on a Bruker Tensor 27 spectrometer with KBr as a diluting reagent. Raman spectrophotometry was recorded on a T64000 HORIBA Jobin–Yvon spectrometer using an Ar green laser at 514.5 nm. X-ray photoelectron spectroscopy (XPS) was carried out by an Axis Ultra DLD, Kratos Analytical Ltd XPS using Al K_α at 1486.6 eV as an excitation source and C $1s$ at 285.1 eV as a standard.

Photocatalytic activity was evaluated through the degradation of rhodamine B (RhB) as a model dye solution. Then 0.2 g photocatalyst was added to 1×10^{-5} M of 200 mL RhB solution which was magnetically stirred to form homogeneous solution in the dark for 30 min for adsorption–desorption equilibrium. Under visible light irradiation, RhB solution was sampled for every 30 min and centrifuged. The residual RhB was measured by a UV–visible spectrophotometer (Perkin Elmer, Lambda 25 spectrometer) at λ_{max} of 554 nm. The photodegradation of RhB was calculated using the below equation.

$$\text{Decolorization efficiency } (\%) = (1 - C_t/C_o) \times 100, \tag{1}$$

where C_o is the initial concentration of RhB at adsorption–desorption equilibrium and C_t is the concentration of RhB after visible light irradiation within the elapsed time (t).

RESULTS AND DISCUSSION

Phase of the samples synthesized by PVP-assisted hydrothermal method at 180°C for 24 h was investigated by XRD. XRD patterns of all samples synthesized using different PVP 10 kDa contents (Fig. 1) were identified to pure tetragonal BiOBr phase (JCPDS No. 09-0393 [25]). Diffraction of the (001) (002), (101), (102), (110), (003), (111), (112), (103), (004), (200), (113), (201), (104), (211), (114), (212) and (203) planes of tetragonal BiOBr phase was detected at 2θ of 10.94°, 22.02°, 25.24°, 31.80°, 32.31°, 33.29°, 34.27°, 39.44°, 40.57°, 44.64°, 46.32°, 46.88°, 47.72°, 50.83°, 53.47°, 56.13°, 57.25° and 58.23°, respectively. No diffraction peaks of impurities were detected in the patterns. The results certify that the products are high purified phase of tetragonal BiOBr. All XRD patterns appear as sharp and strong diffraction peaks, implying that all samples have high degree of crystallinity. Upon increasing the content of PVP 10 kDa, the relative intensity of the (00c) planes such as (001) and (002)

Synthesis of Hierarchical BiOBr Nanostructure Flowers by PVP-Assisted Hydrothermal Method and Their Photocatalytic Activities
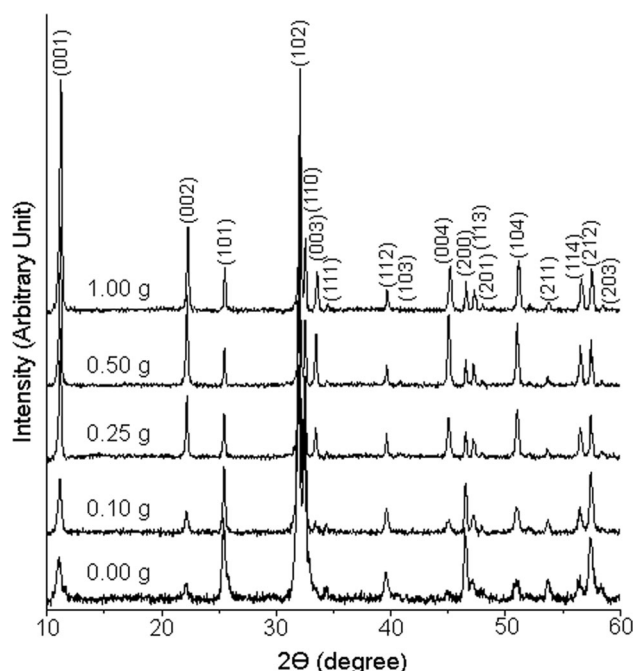
8033

Fig. 1. XRD patterns of BiOBr synthesized in different solutions containing 0.00 g, 0.10 g, 0.25 g, 0.50 g and 1.00 g of PVP 10 kDa by hydrothermal method.

Fig. 2. (a) FTIR and (b) Raman spectra of BiOBr synthesized in the solution containing 1.00 g of PVP 10 kDa by hydrothermal method.

is increased, certifying that the BiOBr sample has a highly preferred orientation in the (001) face.[1,26,27]

Figure 2a shows FTIR spectrum of BiOBr in the wavenumber range of 400–4000 cm^{-1}. The FTIR bands below 1000 cm^{-1} correspond to the Bi-O symmetric stretching vibration. The sharp FTIR bands at 513 cm^{-1} and 730 cm^{-1} are attributed to the Bi-O stretching vibrations.[8,13,26,28]

The vibrational modes of BiOBr with P4/nmm space group are described as $2A_{1g} + B_{1g} + 3E_g + 2E_u + 2A_{2u}$.[18,19] The A_{1g}, B_{1g} and E_g are Raman active, and the E_u and A_{2u} are IR active.[29,30] Figure 2b shows Raman spectrum of BiOBr in the wavenumber range of 50–500 cm^{-1}. Three Raman peaks were detected at 58 cm^{-1}, 113 cm^{-1} and 159 cm^{-1} which correspond to the external A_{1g}, internal A_{1g}, and E_{1g} internal Bi-Br stretching modes, respectively.[26,29,30] The Raman peak at 90 cm^{-1} is assigned to be the Bi-Br stretching mode.[26,29]

XPS analysis is used to explain surface element and valence state of BiOBr as the results shown in Fig. 3. The XPS survey spectrum of BiOBr indicates that the as-synthesized BiOBr sample is composed of Bi, O and Br. Two high-resolution XPS peaks of Bi 4f were detected at 159.3 eV and 164.6 eV corresponding to Bi $4f_{7/2}$ and Bi $4f_{5/2}$, respectively.[2,7,8,26] The difference in binding energy of Bi 4f is 5.3 eV, which indicates the presence of Bi species as trivalent ions in the BiOBr sample.[31,32] The O 1s shows three Gaussian peaks at 530.4 eV, 53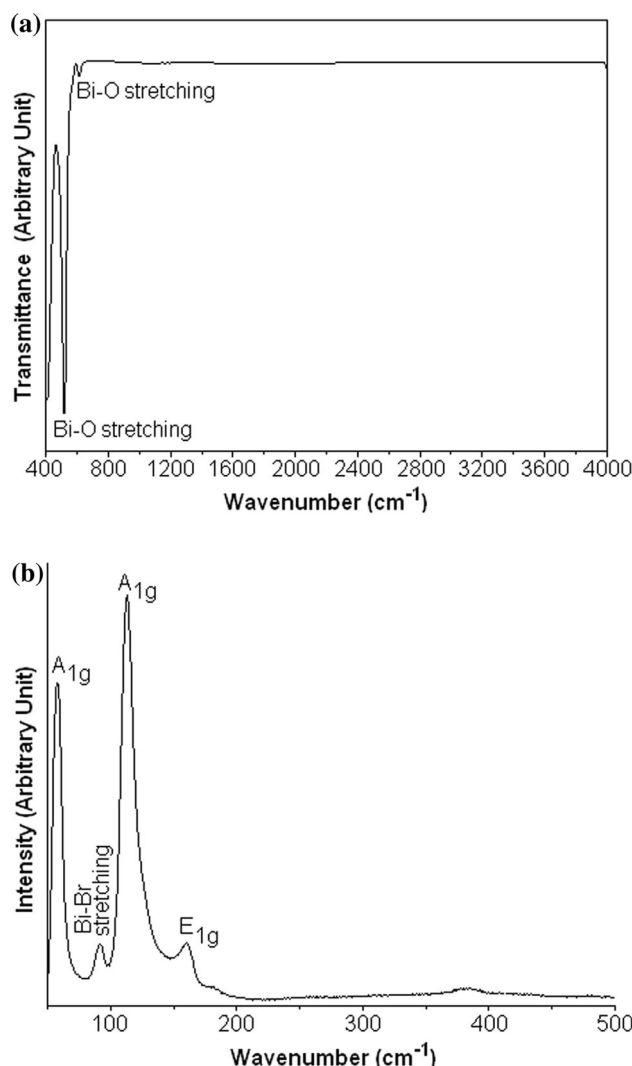1.99 eV and 533.0 eV. They correspond with oxygen of $[Bi_2O_2]^{2+}$ chemical bonding in BiOBr, and O-H and C-O of adsorbed H_2O and CO_2 on surface of BiOBr sample.[2,8,26] XPS spectrum of Br 3d shows two strong binding-energy peaks at 68.3 eV and 69.8 eV which are assigned to Br $3d_{5/2}$ and Br $3d_{3/2}$ of Br$^-$ anions in BiOBr sample, respectively.[2,7,8,26]

Morphologies of BiOBr synthesized in the solutions containing 0.00 g, 0.10 g, 0.25 g, 0.50 g and 1.00 g of PVP 10 kDa and 1.00 g PVP 35 kDa were characterized by SEM as the results shown in Fig. 4. In this research, uniform square BiOBr nanoplates with edge length of 1–3 μm were obtained by hydrothermal reaction at 180°C for 24 h without PVP adding. No other morphologies were produced. The surface of square BiOBr nanoplates is smooth. When 0.10 g PVP 10 kDa with a molecular weight of 10,000 was added, the uniform square BiOBr nanoplates were transformed into irregular BiOBr nanoplates with size of 1–3 μm in diameter. In a solution containing
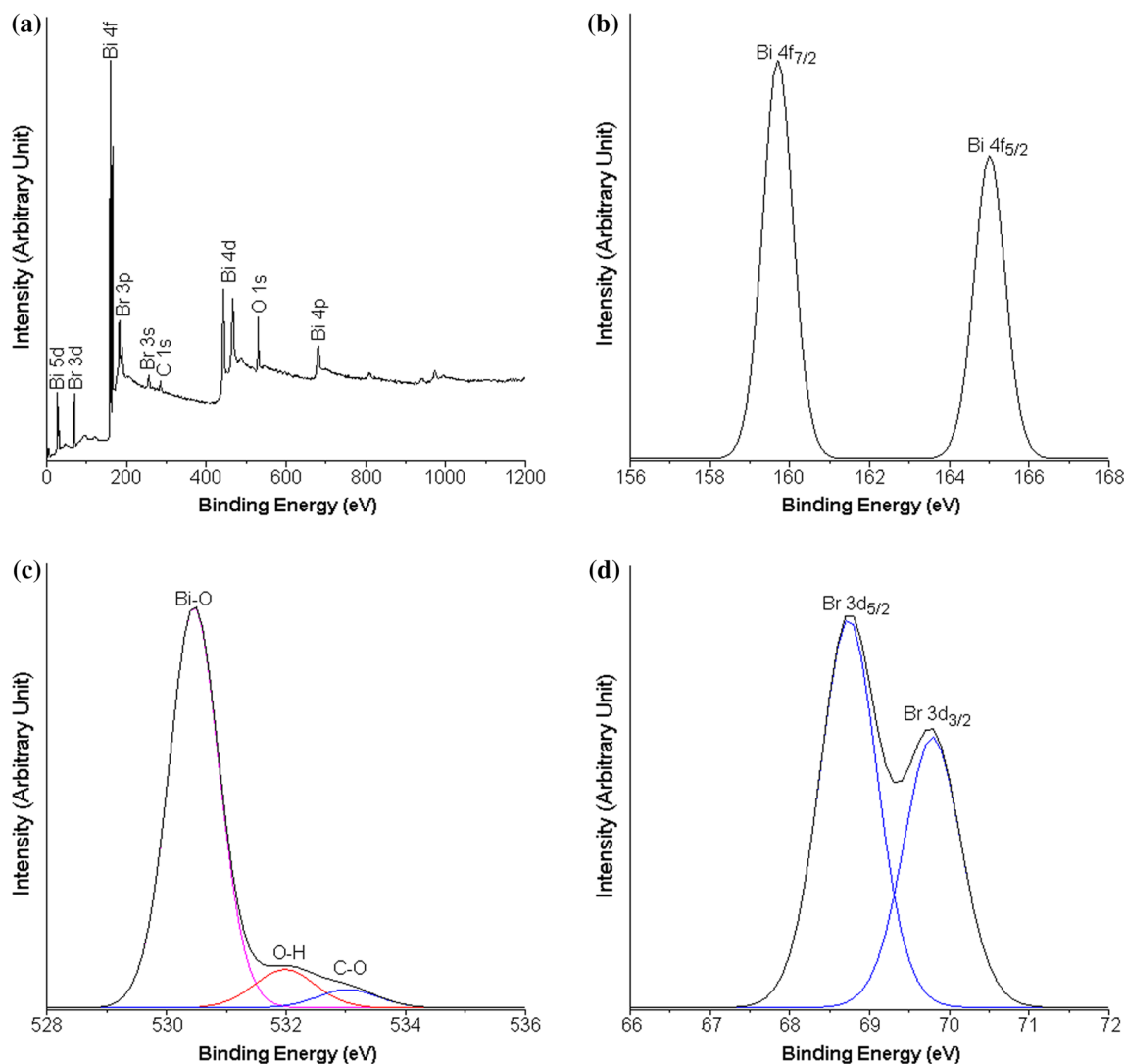
(a)

(b)

(c)

(d)

Fig. 3. XPS spectra of (a) full scan, (b) Bi 4*f*, (c) O 1*s* and (d) Br 3*d* of BiOBr synthesized in the solution containing 1.00 g of PVP 10 kDa by hydrothermal method.

0.25 g of PVP 10 kDa, mixed morphologies of irregular nanoplates as a majority and hierarchical nanostructure flowers as a minority were detected. Some irregular BiOBr nanoplates began to form self-assembled BiOBr nanoplates appearing as hierarchical nanostructure flowers with nanoplates as petals. The hierarchical BiOBr nanostructure flowers were built by connecting each of other nanoplates around a center. When 0.50 g PVP 10 kDa with the same molecular weight was used, complete hierarchical BiOBr nanostructure flowers with different sizes were produced. In the end, uniform hierarchical BiOBr nanostructure flowers with size of 3–4 μm were produced in the solution containing 1.00 g PVP 10 kDa. Clearly, BiOBr flowers are hierarchically assembled by numerous nanosheets. The nanopetals are $\sim$ 10 nm thick and $\sim$ 200 nm long. This open BiOBr structure with less dense nanosheets is expected to contribute large specific surface area and excellent photocatalytic properties.

Upon changing the PVP 10 kDa to PVP 35 kDa, the hierarchical nanostructure flowers were broken into thin microplates. Thus the hierarchical BiOBr microflowers were successfully synthesized in the solution containing 1.00 g PVP 10 kDa by the hydrothermal method.

Figure 5 shows TEM images and SAED patterns of as-synthesized BiOBr in the solutions containing different contents of PVP 10 kDa by the hydrothermal method. The TEM image of pure BiOBr sample clearly shows that the product without PVP adding is composed of square BiOBr nanoplates. Its SAED pattern appears as white spots in systematic arrays, demonstrating that an individual square BiOBr nanoplate is single crystal. The pattern can be indexed to the (110), (200) and (1–10) planes of tetragonal BiOBr with zone axis of [00–1]. It certifies that square nanoplates prefer to grow along the c-axis. The square nanoplates are composed of the $\pm$ (100) top and bottom faces, and
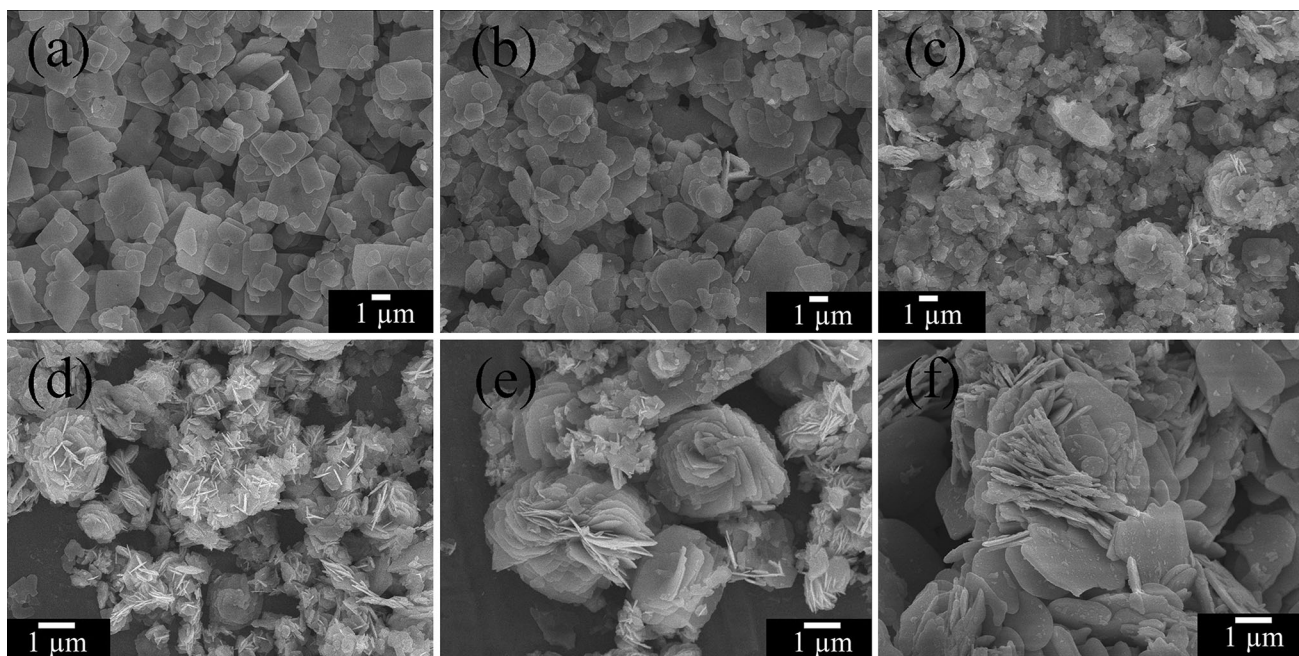
Fig. 4. SEM images of BiOBr synthesized by PVP-assisted hydrothermal method using (a) 0.00, (b) 0.10, (c) 0.25, (d) 0.50 and (e) 1.00 g of PVP 10 kDa, and (f) 1.00 g of PVP 35 kDa.
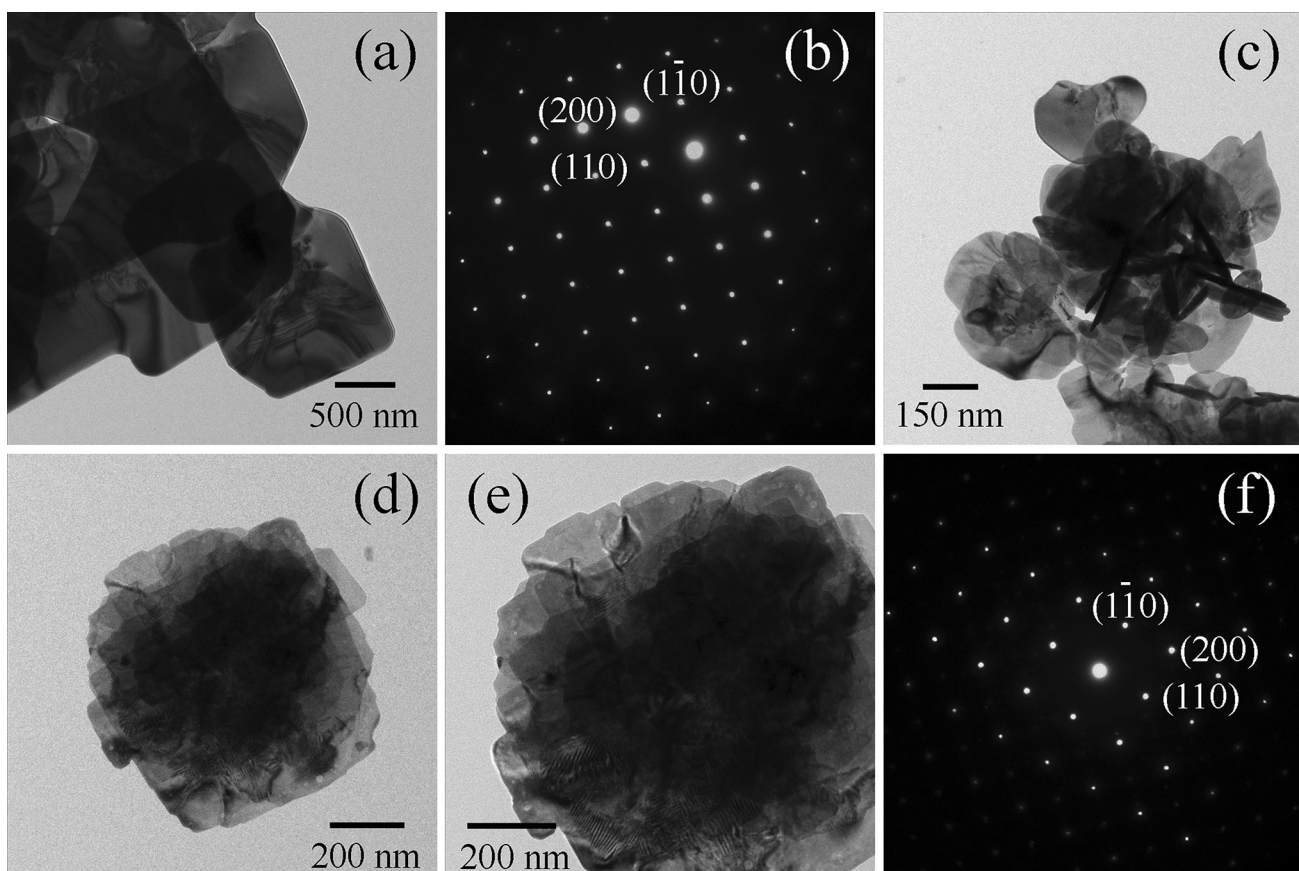

Fig. 5. TEM and HRTEM images, and SAED patterns of the BiOBr samples synthesized by PVP-assisted hydrothermal method using (a and b) 0.00 g, (c) 0.25 g, and (d–f) 1.00 g of PVP 10 kDa.

$\pm$ (110) side and end faces. Upon adding with 0.25 g PVP 10 kDa, the BiOBr nanoplates start to form self-assembled structured flowers. These BiOBr structured flowers are composed of poorly packed nanosheets of multilayered structure. In the solution containing 1.00 g PVP 10 kDa, the as-synthesized BiOBr sample is composed of three-dimensional mutual-connecting flowers composing crystalline nanoplates with the formation of 100–200 nm diameter petals. According to the high magnification image of hierarchical nanostructure flowers, a large amount of stacked nanoplates with smooth surface clusters together in groups of spherical flowers. A SAED pattern of a single nanoplate of hierarchical nanostructure flowers is composed of bright diffraction spots, indicating that the product is a single crystal. There were the detection of the (110), (2 00) and (1–10) planes of tetragonal BiOBr projected along the [001] zone axis which is parallel to the growth direction of the corresponding BiOBr nanoplate. The analysis indicates that the nanoplate petals of hierarchical nanostructure flowers preferentially grow along the c-axis.

The formation mechanism of hierarchical BiOBr nanostructure flowers is schematically shown in Fig. 6. To form hierarchical BiOBr nanostructure flowers, free Bi^{3+} ions react with free Br^{-} ions in the aqueous solution containing dissolved oxygen to form BiOBr nuclei under hydrothermal condition. The BiOBr nuclei grow to form small nanoplates due to the intrinsic tetragonal layer-structure with $[Bi_2O_2]^{2+}$ slabs interleaved by double slabs of Br^{-} ions.[22,33–35] At this stage, the PVP 10 kDa is adsorbed on the surface of small BiOBr nanoplates. Thus, the growth of small BiOBr nanoplates to large BiOBr nanoplates is inhibited.[22,33,36] Subsequently, the small BiOBr nanoplates are self-assembled into

structured flowers because of the reduction of surface free energy. The self-assembled BiOBr structured flowers grow to form hierarchical BiOBr nanostructure flowers through the Ostwald ripening process.[33,36] The hierarchical BiOBr nanostructure flowers are built by bonding each of other nanoplates around a center. Thus the PVP 10 kDa plays an important role in forming hierarchical BiOBr nanostructure flowers.

The photocatalytic activities of as-prepared BiOBr nanostructure synthesized in the solution containing different contents of PVP 10 kDa were studied for RhB photodegradation under visible light irradiation ($\lambda \geq 420$ nm). Figure 7a shows the decrease of absorption spectra of RhB solution over hierarchical nanostructure flowers versus irradiation time. The pink RhB solution was changed to colorless and transparent solution upon illumination with visible radiation for 180 min. The results demonstrate that RhB is completely degraded by hierarchical BiOBr nanostructure flowers. The maximum absorption peak of RhB at 554 nm is gradually decreased with increasing in the irradiation time. The absorption shows blue-shift to shorter wavelength due to the de-ethylation of RhB to rhodamine at 498 nm.[37,38]

Figure 7b shows photocatalytic performance of BiOBr synthesized in the solutions containing different contents of PVP 10 kDa and 1.00 g PVP-35 kDa for photodegradation of RhB under visible light with respect to that of the blank RhB solution. Obviously, pure RhB solution without photocatalyst is of very high stability under visible light illumination. This test indicates that RhB molecules were not degraded by the visible light. The photocatalytic performance of as-synthesized BiOBr for photodegradation of RhB under visible light is
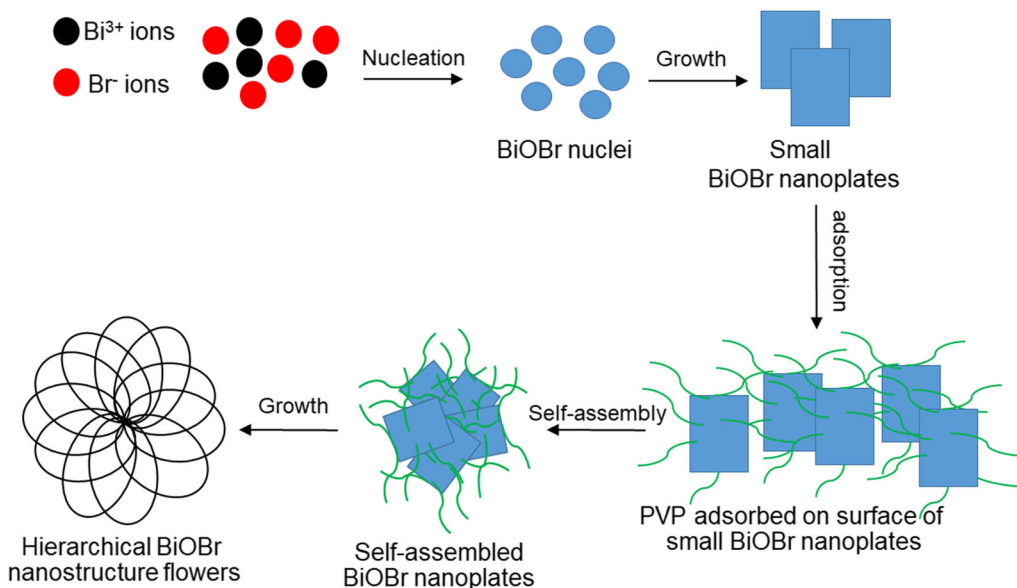

Fig. 6. Schematic diagram for formation mechanism of hierarchical BiOBr nanostructure flowers.
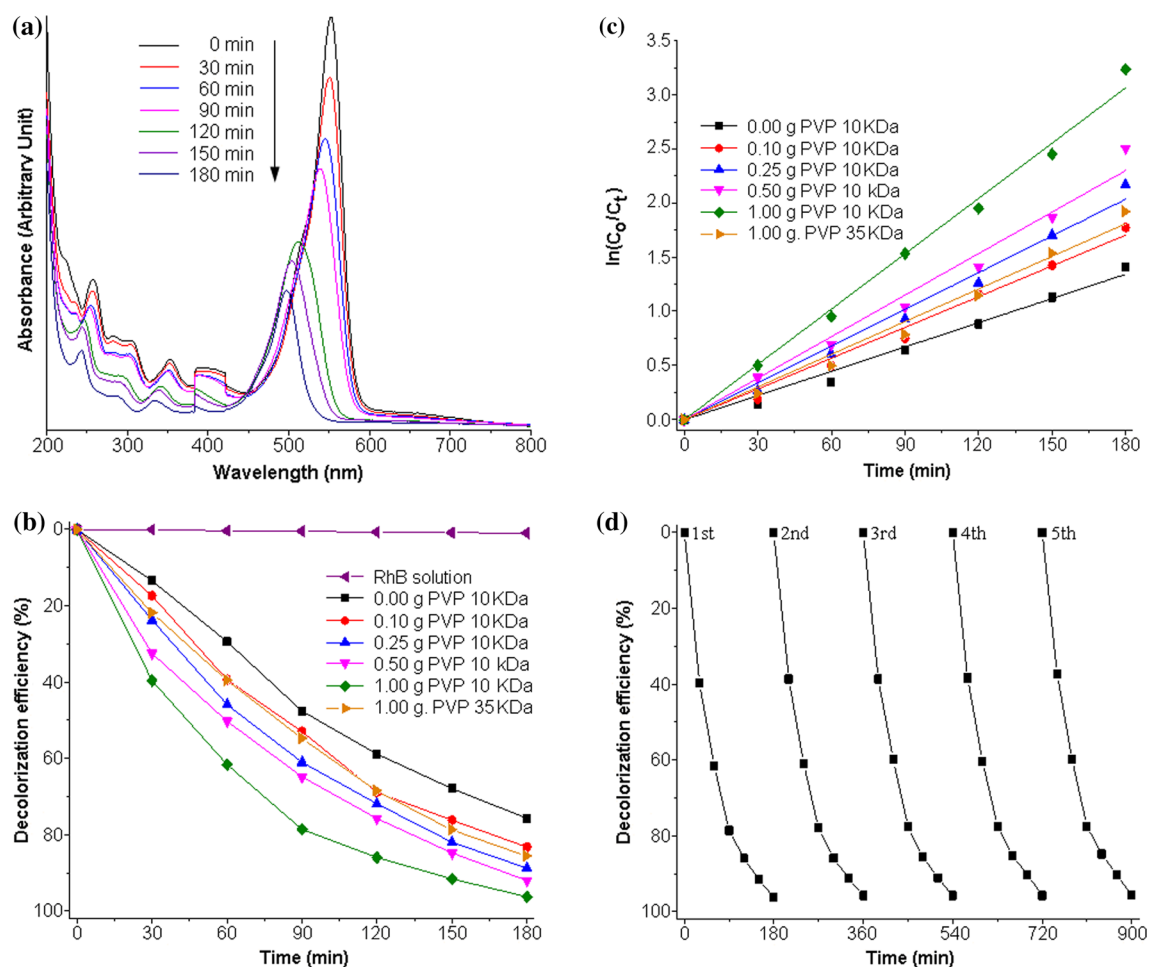
Synthesis of Hierarchical BiOBr Nanostructure Flowers by PVP-Assisted Hydrothermal Method and Their Photocatalytic Activities

8037

Fig. 7. (a) UV–visible absorption of RhB over BiOBr synthesized in the solution containing 1.00 g of PVP 10 kDa under visible light irradiation for different lengths of reaction time. (b) Decolorization efficiency and (c) pseudo-first-order plot for photocatalytic degradation of RhB by BiOBr synthesized in the solutions containing 0.00 g, 0.10 g, 0.25 g, 0.50 g and 1.00 g of PVP 10 kDa, and 1.00 g of PVP 35 kDa with respect to the decolorization efficiency of the blank. (d) Recyclability for photodegradation of RhB by BiOBr synthesized in the solution containing 1.00 g of PVP 10 kDa by hydrothermal method.

influenced by different contents of PVP 10 kDa adding to the precursor solution. At the end of 180 min of photocatalytic test, 75.55%, 83.11%, 86.63%, 91.87%, 96.10% and 85.42% of RhB solution were degraded by BiOBr synthesized in different solutions containing 0.00 g, 0.10 g, 0.25 g, 0.50 g and 1.00 g of PVP 10 kDa, and 1.00 g of PVP 35 kDa, respectively. Thus, hierarchical BiOBr nanostructure flowers improve photodegradation of RhB under visible light, and are attributed to large active specific surface areas. Under visible light irradiation, the photogenerated electrons are excited from the valence band to the conduction band of BiOBr with holes generated in the valence band. The photogenerated electrons and holes diffuse to the BiOBr surface and react with the adsorbed O_2 and OH^-/H_2O to produce $\cdot O_2^-$ and $\cdot OH$ as active oxidizing species on a BiOBr surface.[2,30,37] Both $\cdot O_2^-$ and $\cdot OH$ radicals are strong oxidizing species which can transform RhB molecules into CO_2 and H_2O as final products. Thus, the photo-induced electron–hole pairs are effectively

separated and are mainly responsible for enhanced photocatalytic activity of hierarchical BiOBr nanostructure flowers because the photogenerated electron–hole recombination rate is reduced.[12,13,39]

The pseudo-first-order model of photodegradation of RhB was used to investigate the photocatalytic performance of BiOBr synthesized in the solutions containing 0.00 g, 0.10 g, 0.25 g, 0.50 g and 1.00 g of PVP 10 kDa, and 1.00 g of PVP 35 kDa by the hydrothermal method. Figure 7c is the plot of linear lines of $\ln(C_o/C_t)$ versus irradiation time photodegradation of RhB by the as-synthesized BiOBr with different contents of PVP of 10 kDa and 35 kDa adding in the precursor solutions. The linearity indicates that photocatalytic reaction follows the pseudo-first-order model.[1,3,37,38] The photocatalytic degradation constants of RhB over the photocatalysts are 0.0074 min^{-1}, 0.0094 min^{-1}, 0.0113 min^{-1}, 0.0128 min^{-1}, 0.0171 min^{-1} and 0.0101 min^{-1} for BiOBr synthesized in the solutions containing 0.00 g, 0.10 g, 0.25 g, 0.50 g and 1.00 g of PVP 10 kDa, and 1.00 g of PVP 35 kDa,

respectively. Thus, the hierarchical BiOBr nanostructure flowers have the highest degradation efficiency due to the highest active specific surface area on hierarchical nanostructure flowers for absorbing of visible light and producing $\cdot O_2^-$ and $\cdot OH$ active oxidizing species.[12,13,37,39]

The stability of the hierarchical BiOBr nanostructure flowers was studied through the reused hierarchical BiOBr nanostructure flowers for photodegradation of RhB under visible-light irradiation ($\lambda > 420$ nm) at the same RhB concentration as the results shown in Fig. 7d. At the end of each run, the recycled photocatalyst was separated by centrifugation, washed with water and ethanol, and dried prior to the next run. At the end of the fifth run, the photocatalytic activity of hierarchical BiOBr nanostructure flowers still retains almost 95%, suggesting that the hierarchical BiOBr nanostructure flowers has excellent photodegradation stability.

CONCLUSIONS

In this research, BiOBr was successfully synthesized as visible-light-driven hierarchical nanostructure flowers by a PVP-assisted hydrothermal method. The content of PVP 10 kDa is a key parameter used to control the morphologies of tetragonal BiOBr structure. The morphology of as-synthesized BiOBr without PVP addition appears as uniform square BiOBr nanoplates. In the solution containing 1.00 g of PVP 10 kDa, the square nanoplates transformed into hierarchical nanostructure flowers. Under visible light irradiation, the hierarchical BiOBr nanostructure flowers show the highest photodegradation of RhB of 96.10% within 180 min.

ACKNOWLEDGMENTS

REFERENCES

1. G. Cao, Z.S. Liu, P.Z. Feng, Y.L. Zhao, and J. Niu, *Mater. Chem. Phys.* 199, 131 (2017).
2. A.M. Alansi, M. Al-Qunaibit, I.O. Alade, T.F. Qahtan, and T.A. Saleh, *J. Mol. Liq.* 253, 297 (2018).
3. R. Li, X. Gao, C. Fan, X. Zhang, Y. Wang, and Y. Wang, *Appl. Surf. Sci.* 355, 1075 (2015).
4. R. Shahbazi, A. Payan, and M. Fattahi, *J. Photochem. Photobiol. A* 364, 564 (2018).
5. M. Pirhashemi, A. Habibi-Yangjeh, and S.R. Pouran, *J. Ind. Eng. Chem.* 62, 1 (2018).
6. M. Cheng, G. Zeng, D. Huang, C. Lai, P. Xu, C. Zhang, and Y. Liu, *Chem. Eng. J.* 284, 582 (2016).
7. P. Wang, P. Yang, Y. Bai, T. Chen, X. Shi, L. Ye, and X. Zhang, *J. Taiwan Inst. Chem. Eng.* 68, 295 (2016).
8. S. Yin, W. Fan, J. Di, T. Wu, J. Yan, M. He, J. Xia, and H. Li, *Colloids Surf. A* 513, 160 (2017).
9. H.T. Wang, M.S. Shi, H.F. Yang, N. Chang, H. Zhang, Y.P. Liu, M.C. Lu, D. Ao, and D.Q. Chu, *Mater. Lett.* 222, 164 (2018).
10. Y. Miao, Z. Lian, Y. Huo, and H. Li, *Chin. J. Catal.* 39, 1411 (2018).
11. W. Li, Y. Zou, X. Geng, F. Xiao, G. An, and D. Wang, *Mol. Catal.* 438, 19 (2017).
12. J. Xia, S. Yin, H. Li, H. Xu, L. Xu, and Y. Xu, *Dalton Trans.* 40, 5249 (2011).
13. H. Patnam, L.K. Bharat, S.K. Hussain, and J.S. Yu, *J. Alloys Compd.* 763, 478 (2018).
14. M. Hu, A. Yan, X. Wang, F. Huang, Q. Cui, F. Li, and J. Huang, *Mater. Res. Bull.* 116, 89 (2019).
15. J. Lyu, Z. Hu, Z. Li, and M. Ge, *J. Phys. Chem. Solid.* 129, 61 (2019).
16. L. Ye, Y. Su, X. Jin, H. Xie, F. Cao, and Z. Guo, *Appl. Surf. Sci.* 311, 858 (2014).
17. E.L. Cuellar, A.M. Cruz, N.C. Torres, and J.O. Cortez, *Catal. Today* 252, 2 (2015).
18. E.L. Cuellar, J.O. Cortéz, A.M. Cruz, A.G. Loera, and U.O. Méndez, *Thin Solid Films* 659, 57 (2018).
19. R. Li, C. Fan, X. Zhang, Y. Wang, Y. Wang, and H. Zhan, *Thin Solid Films* 562, 506 (2014).
20. L. Cheng, X. Hu, and L. Hao, *Ultrason. Sonochem.* 44, 137 (2018).
21. K. Gao, X. Bai, Y. Zhang, and Y. Ji, *Electrochim. Acta* 318, 422 (2019).
22. T. Thongtem, A. Phuruangrat, and S. Thongtem, *Cryst. Res. Technol.* 44, 865 (2009).
23. Y. Li, Z. Wang, B. Huang, Y. Dai, X. Zhang, and X. Qin, *Appl. Surf. Sci.* 347, 258 (2015).
24. Y. Wang, Q. Yang, X. Wang, J. Yang, Y. Dai, Y. He, W. Chen, and W. Zhang, *Mater. Sci. Eng. B* 244, 12 (2019).
25. Powder Diffract. File, JCPDS-ICDD (Newtown Square, PA, 2001).
26. D. Wu, S. Yue, W. Wang, T. An, G. Li, H.Y. Yip, H. Zhao, and P.K. Wong, *Appl. Catal. B* 192, 35 (2016).
27. Z. Jiang, F. Yang, G. Yang, L. Kong, M.O. Jones, T. Xiao, and P.P. Edwards, *J. Photochem. Photobiol. A* 212, 8 (2010).
28. Z. Chen, J. Zeng, J. Di, D. Zhao, M. Ji, J. Xia, and H. Li, *Green Energy Environ.* 2, 124 (2017).
29. S. Bunda and V. Bunda, *Acta Phys. Pol. A* 126, 272 (2014).
30. Y. Na, Y.I. Kim, D.W. Cho, D. Pradhan, and Y. Sohn, *Mater. Sci. Semicond. Process.* 27, 181 (2014).
31. Y. Liu, S. Yu, Z. Zhao, F. Dong, X.A. Dong, and Y. Zhou, *J. Phys. Chem. C* 121, 12168 (2017).
32. L. Shan, H. Liu, and G. Wang, *J. Nanopart. Res.* 17, 181 (2015).
33. Z.C. Zhu, P. Chen, X.H. Yang, and R.X. Wang, *J. Exp. Nanosci.* 8, 564 (2015).
34. S. Hu, L. Jiang, Y. Tu, Y. Cui, B. Wang, Y. Ma, and Y. Zhang, *J. Taiwan Inst. Chem. Eng.* 86, 113 (2018).
35. C. Liu, Q. Wu, M. Ji, H. Zhu, H. Hou, Q. Yang, C. Jiang, J. Wang, L. Tian, J. Chen, and W. Hou, *J. Alloys Compd.* 723, 1121 (2017).
36. Y. Chen, M. Wen, and Q. Wu, *CrystEngComm* 13, 3035 (2011).
37. P. Intaphong, A. Phuruangrat, S. Thongtem, and T. Thongtem, *Mater. Lett.* 213, 88 (2018).
38. S. Jonjana, A. Phuruangrat, S. Thongtem, and T. Thongtem, *Mater. Lett.* 175, 75 (2016).
39. R. Li, H. Ren, W. Ma, S. Hong, L. Wu, and Y. Huang, *Catal. Commun.* 106, 1 (2018).